Available online at www.sciencedirect.com
SCIENCE DIRECT®
Journal of Magnetism and Magnetic Materials 279 (2004) 103–110
Journal of magnetism and magnetic materials
www.elsevier.com/locate/jmmm

Structural and electrical properties of $Ni_{1-x}Mg_xFe_2O_4$ synthesized by citrate gel process

L. John Berchmans[a], R. Kalai Selvan[a], P.N. Selva Kumar[a,b], C.O. Augustin[a,*]

[a] *Department of Electropyrometallurgy, Central Electrochemical Research Institute, Karaikudi 630 006, India*
[b] *Department of Materials Science, Madurai Kamaraj University, Madurai 625 021, India*

Received 6 November 2003; received in revised form 22 December 2003

Abstract

The structural and electrical properties of magnesium-substituted nickel ferrite having the general formula of $Ni_{1-x}Mg_xFe_2O_4$ ($x = 0, 0.3, 0.6, 0.9$) has been studied as a function of magnesium ion concentration. The materials have been prepared by citrate gel process using metal nitrate salts as a cation precursors and citric acid as gelating agent. The powder X-ray diffraction pattern confirms fcc structure for the synthesized compound. The variation of lattice parameter and the tetrahedral radius increases with increase in Mg^{2+} ion concentration. The AC electrical parameters such as dielectric constant (ε') and loss tangent ($\tan\delta$) for all the systems have been studied as a function of frequency in the range 50 Hz to 10 kHz at room temperature. A maximum DC electrical conductivity of 3.3 S cm^{-1} was obtained at a temperature of 1000°C and a AC electrical conductivity of 10.94×10^{-6}at 10 kHz was observed in the composition $x = 0.6$ i.e. for $Ni_{0.4}Mg_{0.6}Fe_2O_4$ compound which may be due to the maximum Fe^{2+} concentration in the octahedral sites. The dielectric constant follows the Maxwell's–Wagner interfacial polarization and the relaxation peaks were observed in the dielectric loss properties. The FTIR spectra show the characteristic peaks of ferrite sample. The morphological features were studied using scanning electron microscope.

PACS: 75.50.G; 72.80; 61.10.N

Keywords: Ferrites; Citrate gel process; X-ray diffraction; Electrical properties; Microstructure

1. Introduction

Mixed metallic oxides especially spinels having the general formula AB_2O_4 are very promising materials for technological important applications. Spinel type ferrites are commonly used in many electronic and magnetic devices due to their high magnetic permeability and low magnetic losses [1,2], and also used in electrode materials for high temperature applications because of their high thermodynamic stability, electrical conductivity, electrocatalytic activity and resistance to corrosion [3,4].

$NiFe_2O_4$ possesses an inverse spinel structure is a well known magnetic material which has been studied in detail due to their combined properties. Several researchers have studied the structural, electrical and electrochemical properties of pure

*Corresponding author. Tel.: +91-4565-227550; fax: +91-4565-227713.
E-mail address: caugustin@rediffmail.com (C.O. Augustin).

0304-8853/$ - see front matter © 2004 Elsevier B.V. All rights reserved.
doi:10.1016/j.jmmm.2004.01.073

$NiFe_2O_4$ synthesized by conventional ceramic method [5], sol–gel method [6], co-precipitation method [7], self- propagating high temperature synthesis [8] and high energy milling method [9]. Many attempts have been made to study the structural [10–13] magnetic [14–16], dielectric [17–18] and electrical [19,20] properties of rare earth and transition elements substituted in A-site or B-site of $NiFe_2O_4$. Detailed work has not been carried out on the substitution of $NiFe_2O_4$ with Mg^{2+} ion [21]. Hence, considering the importance of the substituted $NiFe_2O_4$ as an electrode material, the synthesis, structural, electrical properties of $Ni_{1-x}Mg_xFe_2O_4$ have been highlighted. Among the preparative routes the citrate gel process [22] has several potential advantages over the other methods for achieving homogeneous mixing of the compounds on the atomic scale, lower processing temperature, high purity of the synthesized materials, and good control of stoichiometry, desired particle size distribution with high surface area and better sinterability.

The present work deals with the synthesis of $Ni_{1-x}Mg_xFe_2O_4$ ($x = 0$, 0.3, 0.6, 0.9) particles via citrate gel process. The phase formation of the synthesized material has been confirmed by X-ray diffraction and Fourier transform infrared spectroscopy. The AC and DC electrical properties were studied and the powder characteristics were investigated by scanning electron microscope.

2. Experimental

Magnesium substituted nickel ferrite was prepared using citrate gel process with appropriate amounts of high purity nickel nitrate, magnesium nitrate, ferric nitrate and citric acid as starting materials. The stoichiometric redox reactions between metal nitrates and citric acid to produce 1 mol of $NiFe_2O_4$ would require 3:1 molar ratios as calculated from the following equation:

$$Ni(NO_3)_2 \cdot 6H_2O + 2Fe(NO_3)_3 \cdot 9H_2O + C_6H_8O_7 \cdot H_2O \rightarrow NiFe_2O_4 + 29H_2O + 4N_2 + 6CO_2 + 5.5O_2. \quad (1)$$

The desired quantities of nitrate salts were dissolved in triple distilled water and required amounts of citric acid were added as chelating agents. Dilute aqueous ammonia was poured slowly into the nitrate–citrate mixture to adjust the pH to 6.5. The mixed solution was heated at about 100°C for 5 h with uniform stirring and evaporated to obtain a highly viscous gel denoted as precursors. The obtained gel was placed in a hot plate maintained at a temperature 300°C, the gel was swelled and ignited with an evolution of large amounts of gaseous products, resulting the desired ferrite in the form of foamy powder. The powder was then pressed at a pressure of 3.5 tons/cm^2 into 1 and 2.5 cm diameter pellets compacted under identical conditions. The pellets were sintered at 1000°C in air for 50 h.

The frequency variations of AC conductivity of all samples were carried out at room temperature from 50 Hz to 10 kHz with the help of computerized LCRTZ systems (VLCRTZ1P-model). For better ohmic contact silver paste was applied to both surfaces of the pellet, before being sandwiched between the two electrodes of sample holder.

DC electrical conductivity was measured as a function of temperature for the sintered specimens using the modified four-probe method. The crystalline phases of the prepared powders were identified by powder X-ray diffraction technique using a X-ray diffractometer Cu-Kα radiation ($\lambda = 0.1542$ nm). The FTIR spectra of the samples were recorded as KBr discs in the range 400–1000 cm^{-1} by using FTIR-Perkin Elmer, UK Paragon-500. Scanning electron microscopy images (SEM) were made using a JEOL (JSM-3.5 CF) instrument.

3. Results and discussion

3.1. Synthesis

Citric acid is a weak acid and has three carboxylic and one hydroxyl group for coordinating metal ions and therefore enhances the homogeneous mixing. During water dehydration it suppresses the precipitation of metal nitrates.

Because it has electronegative oxygen atoms interacting with electropositive metal ions. Therefore at a relatively low temperature the precursors can form a homogeneous single phase. The ammonia is used to adjust the pH for improving the complexation, gel formation and also to improve the solubility of metal ions [23].

3.2. Structural properties

Fig. 1 represents the X-ray powder diffraction patterns of synthesized samples $Ni_{1-x}Mg_xFe_2O_4$ ($x = 0$, 0.3, 0.6, 0.9). All the samples can be indexed as the single-phase cubic spinel structure. The calculated lattice constant (a) values of $NiFe_2O_4$ ($x = 0$) and $Ni_{0.1}Mg_{0.9}Fe_2O_4$ ($x = 0.9$) are 0.833 and 0.838 nm, respectively, which agree with the reported values [8,24]. The intensities of the (2 2 0), (4 4 0) and (5 1 1) planes are more sensitive to the cations on tetrahedral, octahedral and the oxygen ion parameters respectively [25,26]. As reported earlier Mg^{2+} ions have a strong preference to occupy B sites and partially occupy A sites [27] while Ni^{2+} ions occupy only B sites [28]. Table 1 shows the observed intensities of the above three planes. It can be observed that the intensity of the (4 4 0) plane decreases with the addition of Mg^{2+} ion concentration, which infers that the Ni^{2+} has preferentially occupied the B site, i.e. the octahedral site on the (4 4 0) plane. Since the $NiFe_2O_4$ is established to be an inverse spinel structure. The intensity of (2 2 0) plane increases by the continuous addition of Mg^{2+} ions indicating the preferential occupation of A sites. This trend has not been observed for $Ni_{0.1}Mg_{0.9}Fe_2O_4$ owing to the occupation of Mg^{2+} ions at B-sites also, which leads to migration of Fe^{3+} ions from B-sites to A-sites. This structural behavior is similar to $MgFe_2O_4$ having an inverse spinel in which Mg^{2+} ions occupy B sites [29].

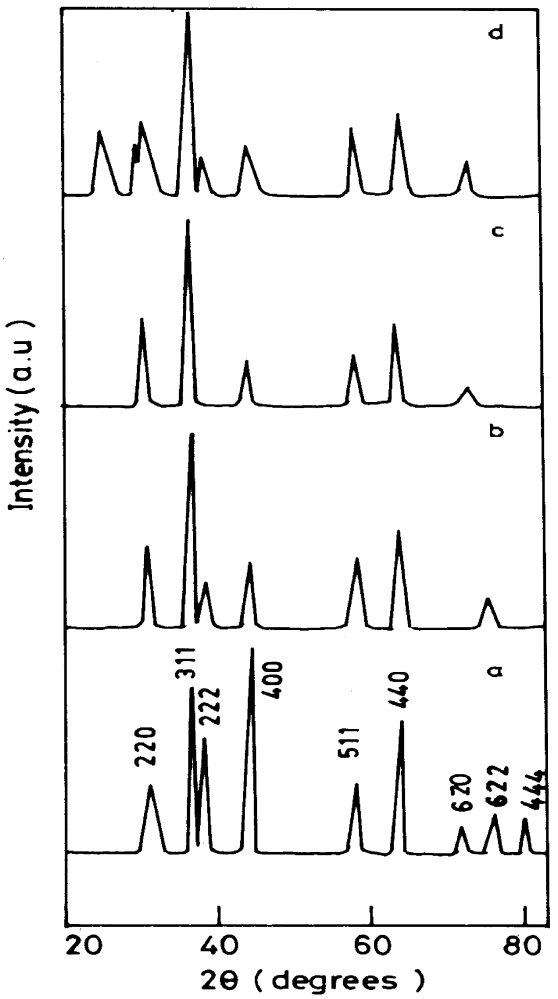

Fig. 1. XRD pattern of $Ni_{1-x}Mg_xFe_2O_4$. (a) $x = 0$, (b) $x = 0.3$, (c) $x = 0.6$, (d) $x = 0.9$.

Fig. 2 shows the variation of lattice constant (a) with increase in Mg^{2+} ion concentration (x). It can be seen that there is an increase of lattice constant with Mg^{2+} ion concentration due to the difference in ionic radii ($Ni^{2+} = 0.69$ Å, $Mg^{2+} = 0.66$ Å, $Fe^{3+} = 0.64$ Å).

Fig. 3 represents the variation of tetrahedral radius with increase in Mg^{2+} concentration, calculated by the following equation:

$$r_{tet} = (1 - x)r_{tet,Fe^{3+}} + (x)r_{tet,Mg^{2+}}. \quad (2)$$

Table 1
Intensity values of *hkl* planes

$Ni_{1-x}Mg_xFe_2O_4$	I_{220}	I_{440}	I_{511}
$x = 0.0$	43	64	44
$x = 0.3$	44	47	40
$x = 0.6$	48	41	35
$x = 0.9$	40	38	35

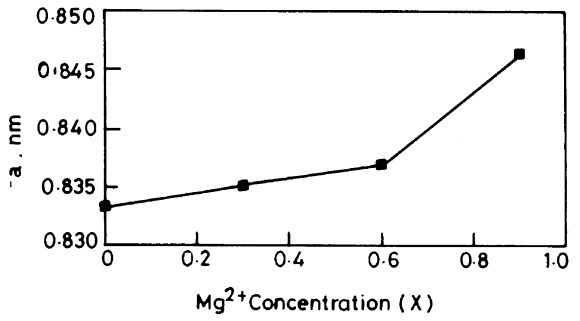

Fig. 2. Lattice constant vs. Mg^{2+} concentration for $Ni_{1-x}Mg_xFe_2O_4$.

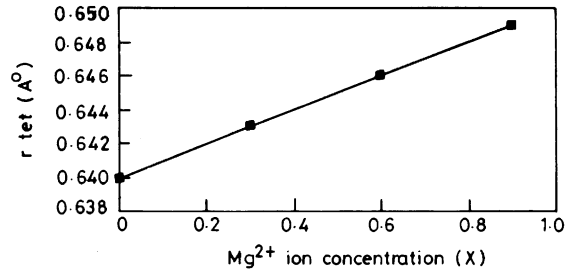

Fig. 3. Tetrahedral radius vs. Mg^{2+} concentration for $Ni_{1-x}Mg_xFe_2O_4$.

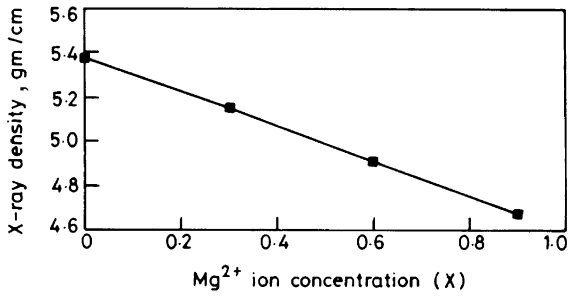

Fig. 4. X-ray density vs. Mg^{2+} concentration for $Ni_{1-x}Mg_xFe_2O_4$.

A linear variation is noticed with substitution of $NiFe_2O_4$ with Mg^{2+} ions.

Fig. 4 explains the variation of X-ray density with influence of Mg^{2+} ion concentration. The X-ray density of the samples has been calculated from the lattice parameters using the formula

$$D_{h\,k\,l} = \frac{8M}{Na^3}, \tag{3}$$

where M is the molecular weight of the sample; N the Avogadro's number and a the lattice parameter of the sample.

From the figure it can be seen that the X-ray density decreases with increase in Mg^{2+} ion content. This may be due to the fact that the density of Mg atom is $1.74\,g/cm^3$ which is lower than that of Ni atom $8.91\,g/cm^3$ as well as the atomic concentration of Mg is less ($4.3\times10^{22}\,cm^{-3}$) compared with Ni concentration ($9.14\times10^{22}\,cm^{-3}$) [30].

The FTIR spectra for the $Ni_{1-x}Mg_xFe_2O_4$ ($x=0$, 0.3, 0.6, 0.9) system were recorded in the range 400–1000 cm^{-1}, which are shown in Fig. 5. The spectra show two main absorption bands v_1 and v_2 corresponding to the stretching vibration of the tetrahedral and octahedral sites around 600 and 400 cm^{-1}, respectively. The spectra for pure $NiFe_2O_4$ show the splitting of absorption bands. The band v_2^* at 419.66 cm^{-1} has a subsidiary band v_2' at 471.87 cm^{-1}. This subsidiary may be due to the Jahn–Teller distortion produced by Fe^{2+} ions which has been reported earlier [31]. The spectra also show a change in shift due to the introduction

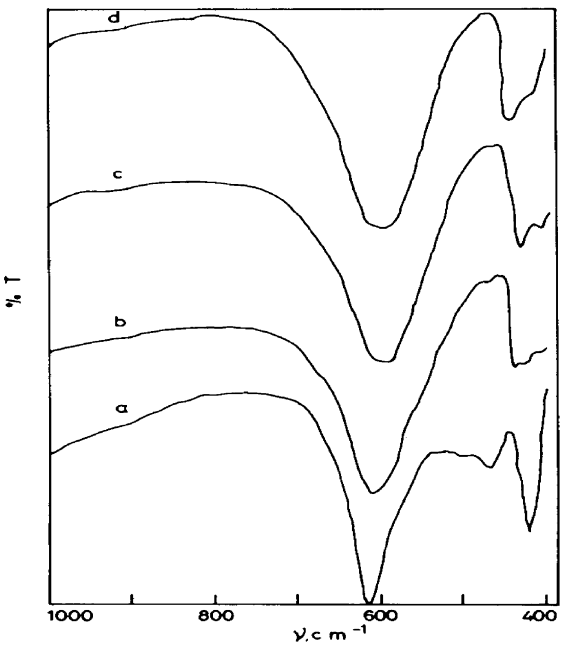

Fig. 5. FTIR pattern of $Ni_{1-x}Mg_xFe_2O_4$. (a) $x=0$, (b) $x=0.3$, (c) $x=0.6$, (d) $x=0.9$.

Table 2
FT–IR parameters

Sites	Band (cm^{-1})	$X = 0$	0.3	0.6	0.9	Me–O^{2-}
Tetrahedral	γ_1^*	613.54	601	591.78	585.41	Fe^{3+}–O^{2-}
Octahedral	γ_2^*	419.66	429.01	432.31	434.34	Ni–O
	γ_{sh}	471.87				
Threshold frequency	γ_{th}	450	460	470	485	
Threshold energy	E_{th} (eV)	0.0563	0.0575	0.0588	0.0607	

of Mg^{2+} ions. The tetrahedral site bands are shifted from higher band values to lower band values i.e. 613.54 to 585.41 cm^{-1}, which can be attributed to the shifting of Fe^{3+} ions towards oxygen ion on occupation of tetrahedral site by Mg^{2+} ions with larger ionic radii, which decreases the Fe^{3+}–O^{2-} distance [32]. The octahedral site bands are shifted from lower to higher values. i.e. 419.66 to 434.74 cm^{-1}. Table 2 shows the band values and the corresponding metal ions. The observed values illustrate that the frequency bands appeared at 417 and 604 $cm^{-1}$are responsible for the formation of $NiFe_2O_4$ [33].

3.3. Electrical properties

In general the electrical properties of the ferrite materials depend upon the method of preparation, chemical composition, grain size and sintering temperature. Fig. 6 illustrates the frequency dependence of the dielectric constant of synthesized materials of $Ni_{1-x}Mg_xFe_2O_4$ ($x = 0$, 0.3, 0.6, 0.9). It can be seen that all the samples show the frequency-dependent phenomena i.e. the dielectric constant decreases with increasing frequency. This is a normal behavior observed in most of the ferrimagnetic materials, which may be due to the interfacial polarization as predicted by Maxwell–Wagner [34]. According to Maxwell–Wagner model, the dielectric structure of a ferrite material is assumed to be made up of two layers. First layer being a conducting layer consists of large ferrite grains and the other being grain boundaries are poor conductor. This bi-layer formation is resulted by high temperature sintering. The polarization results in an electronic exchange between the ferrous and ferric ions, which produce local displacements in the direction of applied external

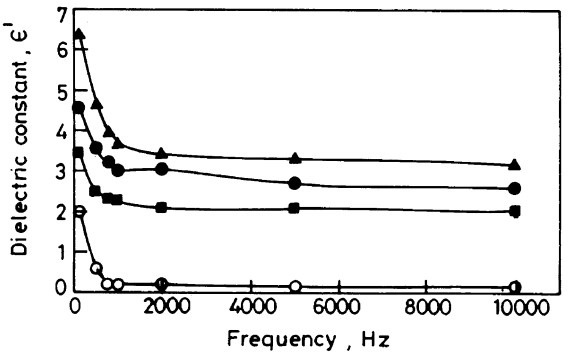

Fig. 6. Plot of dielectric constant vs. frequency for $Ni_{1-x}Mg_xFe_2O_4$ (■) $x = 0$, (●) $x = 0.3$, (▲) $x = 0.6$, (○) $x = 0.9$.

fields. Similarly the $Ni^{3+} \Leftrightarrow Ni^{2+} + e^+$ gives the hole concentration in the octahedral sites which produce the local displacements in the opposite direction of the applied fields. These displacements determine the polarization as well as the dielectric properties. The observed behavior of dielectric constant decrease with increase in frequency is due to the fact that above certain frequencies the electronic exchange between the ferrous and ferric ions does not follow the applied field. The compositional dependence of dielectric constant is also shown in Fig. 6. Among all the specimens the lower dielectric constant value is observed for the $Ni_{0.1}Mg_{0.9}Fe_2O_4$ sample, because of the unavailability of ferrous and ferric ions in the octahedral sites, which are preferentially occupied, by Mg^{2+} ions.

Fig. 7 shows the variation of loss tangent with frequency for the samples of $Ni_{1-x}Mg_xFe_2O_4$ ($x = 0$, 0.3, 0.6, 0.9). It can be seen that an abnormal dielectric behavior was observed for all the samples because the dielectric relaxation peaks are resulted at a frequency of 2 kHz. According to

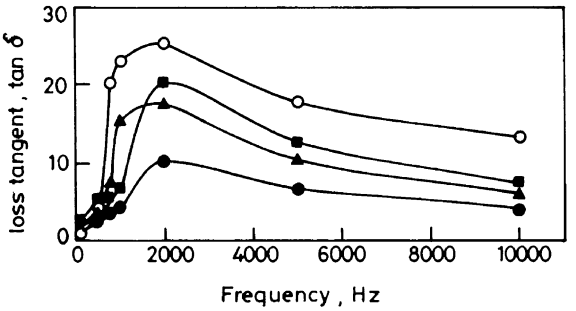

Fig. 7. Plot of loss tangent vs. frequency for $Ni_{1-x}Mg_xFe_2O_4$ (■) $x = 0$, (●) $x = 0.3$, (▲) $x = 0.6$, (○) $x = 0.9$.

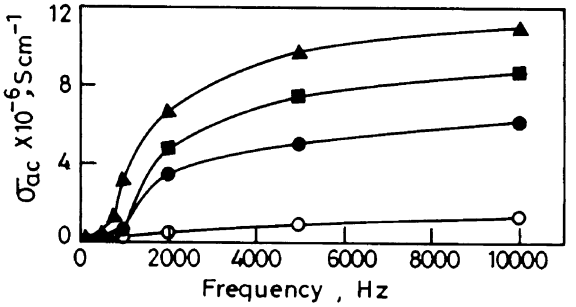

Fig. 8. Plot of AC conductivity vs. frequency for $Ni_{1-x}Mg_xFe_2O_4$ (■) $x = 0$, (●) $x = 0.3$, (▲) $x = 0.6$, (○) $x = 0.9$.

Rezlescu model the relaxation peaks may be due to the collective contribution of both p and n type of charge carriers [35]. The electronic exchange between $Fe^{3+} \Leftrightarrow Fe^{2+}$ and hole transfer between $Ni^{2+} \Leftrightarrow Ni^{3+}$ in octahedral sites are responsible for such behaviors. Furthermore the jumping frequencies of localized charge carriers are almost equal to that of the applied AC electric field.

The frequency dependence of AC electrical conductivity of all the samples is shown in Fig. 8. It is observed that the AC conductivity increases with increasing applied frequency. Since the increase in frequency enhances the hopping frequency of the charge carriers Fe^{2+} and Fe^{3+}, the conduction is increased. The conduction mechanism of ferrite is explained on the basis of hopping of charge carriers between the Fe^{2+} and Fe^{3+} on the octahedral sites. The compositional dependence on AC conductivity also increases with the addition of Mg^{2+} ion in various molar proportions except $Ni_{0.1}Mg_{0.9}Fe_2O_4$.

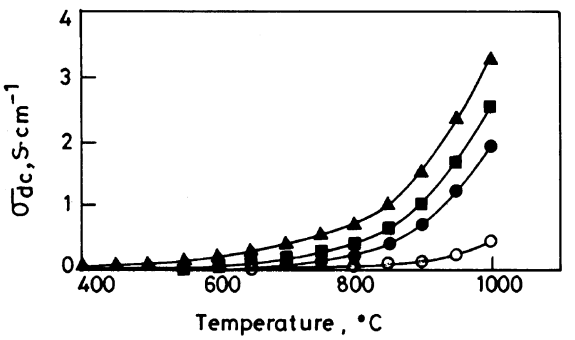

Fig. 9. Plot of DC conductivity vs. temperature for $Ni_{1-x}Mg_xFe_2O_4$ (■) $x = 0$, (●) $x = 0.3$, (▲) $x = 0.6$, (○) $x = 0.9$.

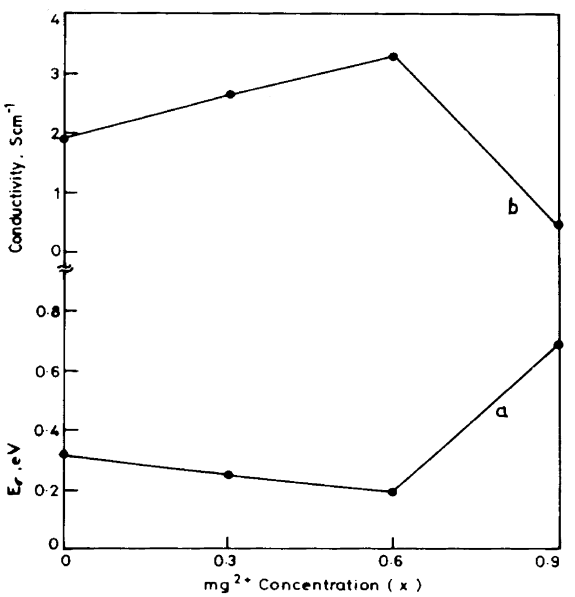

Fig. 10. (a) Plot of activation energy vs. Mg^{2+} ion concentration. (b) Plot of sp. conductivity vs. Mg^{2+} ion concentration.

The relationship between DC conductivity and temperature is shown in Fig. 9. It can be seen that the DC electrical conductivity of the samples increases with the increase in temperature. As the temperature increases the mobility and concentration of the charge carriers increases, therefore the conductivity increases steadily up to 800°C, after which sudden surge in conductivity is observed due to hopping of electrons. Moreover at lower temperature the deleterious effect of some

impurities may reduce conductivity, but at higher temperature this influence becomes negligible. Hence there are two activation energies representing two conducting mechanism. Increase in Mg^{2+} ions concentration also enhances the conductivity up to $x = 0.6$. The conduction mechanism of nickel ferrite can be explained by the following redox reactions:

$$Fe^{2+} \Leftrightarrow Fe^{3+} + e^{-}, \quad (4)$$

$$Ni^{3+} \Leftrightarrow Ni^{2+} + e^{+}. \quad (5)$$

Combining these two equations

$$Ni^{2+} + Fe^{3+} \Leftrightarrow Ni^{3+} + Fe^{2+}. \quad (6)$$

Nickel ferrite has an inverse spinel structure and the cation distribution is as follows $(Fe^{3+})_A$ $[Ni^{2+}Fe^{3+}]_B$ O_4. As the concentration of Mg^{2+} ion in the synthesized material increases some of the Mg^{2+} ions may occupy tetrahedral sites, resulting a migration of Fe^{3+} ions into octahedral sites. The increase in concentration of Fe^{3+} ions at B-sites increases the hopping rate of electrons, which in turn enhances the conductivity to maximum ($3.3\,S\,cm^{-1}$ at $x = 0.6$). In contrast, the lower specific conductivity of $0.8\,S\,cm^{-1}$ obtained for the specimen $Ni_{0.1}Mg_{0.9}Fe_2O_4$ may be due to the unavailability of ferrous and ferric ions at B-sites.

Fig. 10 represents the variation of activation energy and specific conductivity measured at 1000°C with Mg^{2+} ion concentration. From the figure it is found that the activation energy decreases with the increase in concentration of

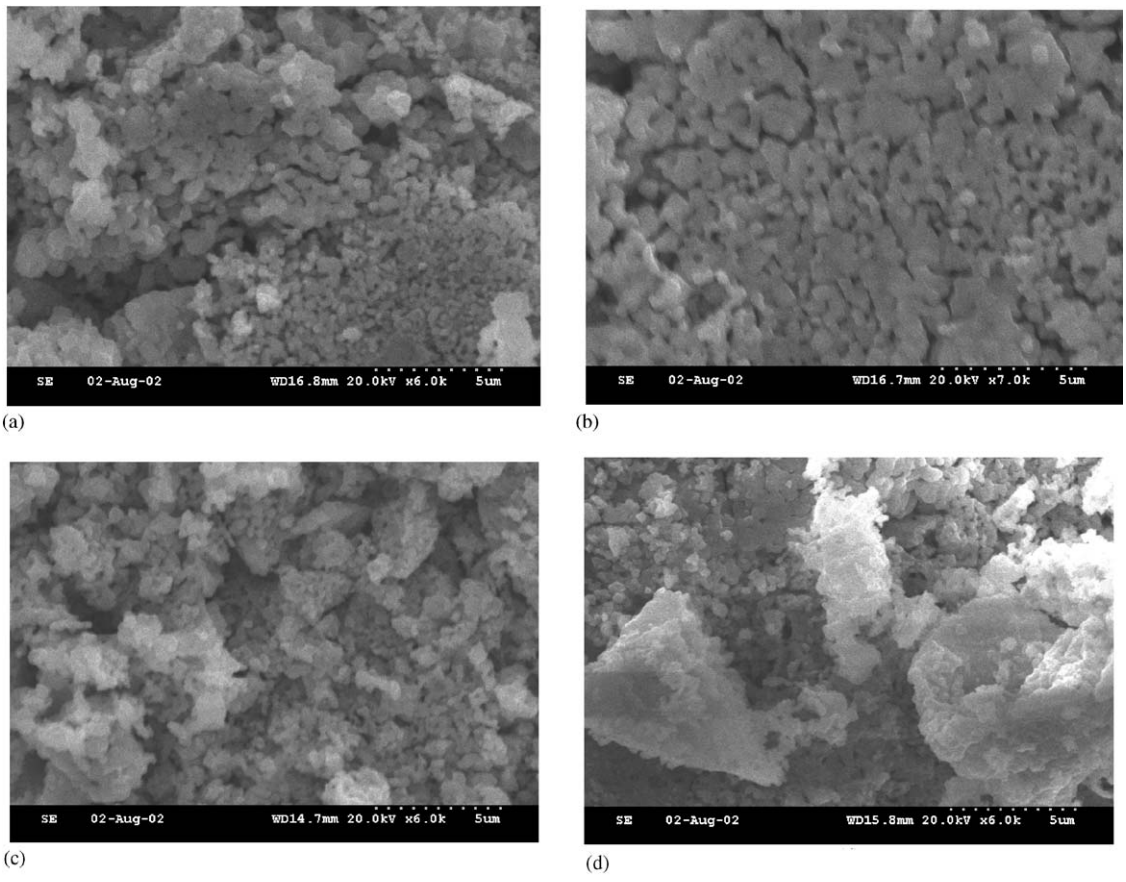

Fig. 11. SEM micrographs of $Ni_{1-x}Mg_xFe_2O_4$. (a) $x = 0$, (b) $x = 0.3$, (c) $x = 0.6$, (d) $x = 0.9$.

Mg^{2+} ions up to $x = 0.6$, whereas in the case of $x = 0.9$ the activation energy is at its maximum causing a lower conductivity. In $Ni_{0.4}Mg_{0.6}Fe_2O_4$ the activation energy will be decreased because the energy required for electron hopping between Fe^{2+} and Fe^{3+} is lower, which corresponds to high conduction.

Fig. 11a–d depicts the scanning electron micrographs of the $Ni_{1-x}Mg_xFe_2O_4$ ($x = 0$, 0.3, 0.6, 0.9) samples. These micrographs reflect agglomerated, well-defined particles with inhomogeneous grain size distribution. An enlarged mass of compound formation was observed due to the influence of magnesium ions.

4. Conclusion

In the present study, the mixed ferrites $Ni_{1-x}Mg_xFe_2O_4$ have been successfully synthesized by citrate gel process. The presence of Mg^{2+} ions causes appreciable changes in the structural and electrical properties of the substituted $NiFe_2O_4$. The X-ray powder diffraction patterns reveal fcc structure for the synthesized materials. The FTIR pattern shows the characteristic peaks of ferrite system. A semiconductor behavior is inferred in the samples, as observed from the electrical conductivity measurements. Similarly ultra fine crystals are revealed from the SEM studies.

Acknowledgements

The authors express their gratitude to The Director, CECRI and staff, Dept. of Materials Science, Madurai Kamaraj University for their kind help.

References

[1] Toshiyuki Suzuki, Termitsu Tanaka, Kaoru Ikemizu, J. Magn. Magn. Mater. 235 (2001) 159.
[2] T. Giannakopoulou, L. Kompotiatis, A. Kontogeorgakos, G. Kordas, J. Magn. Magn. Mater. 246 (2002) 360.
[3] E. Olsen, J. Thonstad, J. Appl. Electrochem. 29 (1999) 293.
[4] C.O. Augustin, D. Prabhakaran, L.K. Srinivasan, J. Mater. Sci Lett. 12 (1993) 383.
[5] F. Novelo, R. Valenzuela, Mater. Res. Bull. 30 (1995) 335.
[6] Dong-Hwang Chen, Xin-Rong He, Mater. Res. Bull. 36 (2001) 1369.
[7] Y. Shi, J. Ding, X. Liu, J. Wang, J. Magn. Magn. Mater. 205 (1999) 249.
[8] W.B. Cross, L. Affleck, M.V. Kuznetsov, I.P. Parkin, Q.A. Pankhurst, J. Mater. Chem. 9 (1999) 2545.
[9] V. Sepeclak, D. Baaba, D. Mienert, D. Schultze, F. Krumenich, F.J. Litterst, K.D. Becker, J. Magn. Magn. Mater. 257 (2003) 377.
[10] Chul Sung Kim, Woo Chul Kim, Sung Yong An, Seung Wha Leo, J. Magn. Magn. Mater. 215–216 (2000) 213.
[11] O.M. Hemada, M.Z. Said, M.M. Barakat, J. Magn. Magn. Mater. 224 (2001) 132.
[12] A.S. Albuquerque, J.D. Ardisson, W.A. Macedo, J.L. Lopez, R. Paniago, A.I.C. Persiano, J. Magn. Magn. Mater. 226–230 (2001) 1379.
[13] Xiuling Jiao, Dairong Cheng, Yong Hu, Mater. Res. Bull. 37 (2002) 1583.
[14] C.N. Chinnasamy, A. Naryanasamy, N. Ponpandian, R. Justin Joseyphus, B. Jaydevi, K. Tohjil, K. Chattopadhyay, J. Magn. Magn. Mater. 238 (2002) 281.
[15] K. Kondo, T. Chibo, S. Yamada, J. Magn. Magn. Mater. 254–255 (2003) 541.
[16] M. Hoque, M.D. Amanullah Choudhury, M.D. Fakrhul Isalm, J. Magn. Magn. Mater. 251 (2002) 292.
[17] K. Vijay Kumar, A. Chandra Shekara Reddy, D. Ravinder, J. Magn. Magn. Mater. 263 (2003) 121.
[18] A.M. Abdeen, J. Magn. Magn. Mater. 192 (1999) 121.
[19] A.M. Abdeen, J. Magn. Magn. Mater. 185 (1998) 199.
[20] El-Shabasy, J. Magn. Magn. Mater. 172 (1997) 188.
[21] M.A. El Hiti, M.A. Ahmed, Mater. Sci. Technol. 14 (1998) 19.
[22] R.N. Panda, J.C. Shih, T.S. Chin, J. Magn. Magn. Mater. 257 (2003) 79.
[23] R.D. Purohit, A.K. Tyagi, J. Mater. Chem. 12 (2002) 312.
[24] K.C. Patil, D. Gajapathy, V. Vernekar, Mater. Res. Bull. 17 (1982) 922.
[25] B.P. Ladgaonkar, A.S. Vaingainkar, Mater. Chem. Phys. 56 (1998) 280.
[26] C.S. Narasimhan, C.S. Swamy, Phys. Stat. Sol. (a) 59 (1980) 817.
[27] R. Kulkarni, H. Joshi, Solid State Commun. 53 (1985) 1005.
[28] B.V. Bhise, M.B. Dongar, S.A. Patil, S.R. Sawant, J. Mater. Sci. Lett. 10 (1991) 922.
[29] S.H. Patil, S.I. Patil, S.M. Kadam, B.K. Chougle, J. Magn. Magn. Mater. 110 (1992) 147.
[30] C. Kittel, Introduction to Solid State Physics, 7th Ed., Wiley, New York, p. 24.
[31] V.A. Potakova, N.D. Zverv, V.P. Romanov, Phys. Stat. Sol. (a) 12 (1972) 623.
[32] S.C. Watawe, B.D. Sutar, B.D. Sarwade, B.K. Chougule, Int. J. Inorg. Mater. 3 (2001) 819.
[33] S. Music, D. Balzar, M. Gotic, S. Popovic, S. Dalipi, Croat. Chem. Acta 70 (1997) 719.
[34] K. Wagner, Ann. Phys 40 (1913) 817.
[35] N. Rezlescu, E. Rezlescu, Phys. Stat. Sol (a) 23 (1974) 575.